

NUMERICAL STUDY OF AXISYMMETRIC SUBSONIC TURBULENT FREE JET PROBLEM

Gylles Ricardo Ströher, gylles@ita.br
Cláudia Regina de Andrade, claudia@ita.br
Edson Luiz Zaparoli, zaparoli@ita.br

Instituto Tecnológico de Aeronáutica, End.: Praça Marechal Eduardo Gomes, 50 - Vila das Acácias CEP 12228-900 – São José dos Campos – SP – Brasil

Abstract. Free jets have been of great interest for many engineering applications as in aerodynamic, thermal, chemical and propulsion systems. In the present study axisymmetric compressible turbulent free jet problem is numerically solved. Governing equations (mass conservation, momentum, energy and turbulence model) are discretized employing the volume finite method with a segregated solver and second order discretization approach. Two different turbulence models were tested Spalart-Allmaras and $v2-f$ using the a CFD tool to determine the most suitable model for the compressible free jet problem. Jet flow conditions were: Mach number 0.6, Reynolds $1.7 \cdot 10^6$ and total temperature at nozzle exit 316 K. Computational results for decay velocity for each simulated case were compared with available experimental data. Results obtained from this investigation indicate that the $v2-f$ turbulence model produced better overall results.

Keywords: Subsonic Free Jet, Turbulence Models, CFD tool.

1. INTRODUCTION

Free Jet flow is an essential element in recent traditional, as well high-tech, applications. Its applications could be found in thermal, chemical and propulsion systems. Jets flow is categorized within the class of a free shear flows, as do wakes and shear layers. In general terms, a jet is a stream of air (or other fluid) issuing from an orifice or a nozzle into a quiescent surrounding. Such flows develop without the influence of a wall, in contrast with boundary layers that exist in the vicinity of a solid surface.

The flow structure of a free jet (goal main in this work) is described in Fig. 1. In this case there are three distinct regions in the flow, the potential core and the developed region and region in between named transition region. The potential core is region in the near field of the nozzle exit. In this region, the centerline axial mean velocity is constant. As the shear layers meet, the jet undergoes a transition into the fully developed regime. In the fully developed region, the jet is self similar. This means that profiles of a flow quantity, such as axial mean velocity, taken at different downstream distances, will all collapse when properly scaled. Self similarity, also called self preservation, is a very interesting feature of flows, as flow properties depend on one variable only. The self similar regime is established a few nozzle diameters downstream the nozzle exit, regardless of its initial conditions; though they will influence the location at which the self similar region starts.

The two converging lines in Fig. 1 represent the growing of the shear layers. Their meeting location (x_c) is known as the potential core length and corresponds to the full extent of the first region. The name potential core derives from the fact that in the region defined by these two lines, the axial mean velocity remains constant, as would happen in a potential flow (inviscid and irrotational). In fact, the viscous effects are not felt in the mean flow in this region. Only in the region where shear is high, is viscosity important. Therefore, for $x < x_c$, there are two well defined areas: inside and outside the two converging lines. While remaining constant inside the lines, the axial mean velocity tends asymptotically to zero outside them. For $x > x_c$ there is no longer a region of constant axial mean velocity. As the shear layers have met, mixing now is going on throughout the whole crosswise extent of the jet. As a consequence, the centerline velocity starts decaying with x .

Two and three-dimensional air jets are studied by many researchers both theoretically and experimentally and turbulent jets have been the subject of many experimental and numerical works for over 40 years (Klein et al 2003). Pais and Leland (1996) performed experiments in jet impingement cooling for free and submerged surfaces. Heat transfer and pressure drop data for a wide range of flow field parameters were obtained with a circular jet for different levels of submersion, Reynolds number (range of 100 to 6000), Prandtl number (range of 50 to 470), and jet diameters from 0.5 mm to 1.7 mm. Comparisons of heat-transfer coefficient are presented for free and fully submerged jet cases and showed no significant change in the heat transfer rate based on whether the test surface is free or submerged.

Wishart and Krothapalli (1996) obtained experimental data of a rectangular jet issuing into a parallel free-stream using pitot probe measurements. Emphasis was placed on the effect of the external stream on the global structure of the developing jet. The jet nozzle exit had an aspect ratio of 4 to 1, and the jet exit Reynolds number, based on the short dimension of the nozzle, is $6 \cdot 10^4$. The free-stream to jet exit velocity ratio was varied by changing the free-stream velocity, and ranges from 0 to 0.5. Results indicated that the jet spreads linearly in both the x - y and the x - z planes and that similarity is established at downstream distances of $x/W = 10$ (W is the width of dimension of the jet).

Keysar and Degani (2004) performed numerical simulations of an axisymmetric compressible turbulent jet, using a finite volume commercial CFD solver, implementing Roe's flux-difference-splitting upwind scheme. The turbulent models and numerical method were examined and validated by comparison of computational results to experimental

measurements. These authors showed that for fully-expanded jets accurate calculation of the shear layer formed can be obtained using coarse numerical discretization ($\sim 1,000$ cells with a first order numerical scheme), and an isotropic two equation $k-\varepsilon$ turbulence model. On the other hand, for nonexpanded jets, when the shear layer interacts with shock waves and expansion fans, achieving accurate results requires the use of fine numerical discretization ($\sim 100,000$ cells with a second order numerical scheme), and the non-isotropic four-equation RSM turbulence model. For highly underexpanded jets with Mach disks, the solution could not be converged with the RSM model. However, satisfactory results were obtained with the RNG $k-\varepsilon$ model.

In the present work, two turbulence models were tested using the CFD software Fluent (Release 6.2) to study the subsonic free jet problem. The jet flow was at Mach number of 0.6, $Re\ 1.7 \cdot 10^6$ and total temperature at nozzle exit 316 K. The turbulence models examined were: Spalart-Allmaras (Spalart and Allmaras, 1992) and $v2-f$ (Durbin, 1995). The computational results of decay velocity for each case were compared with the experimental data.

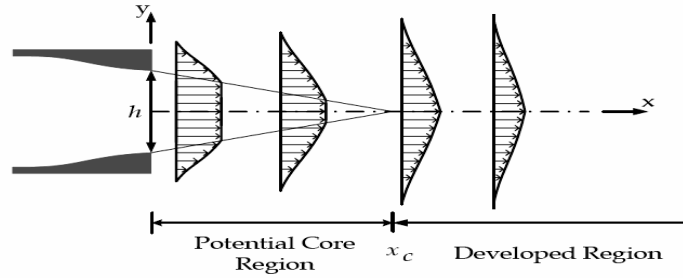


Figure 1. Structure of free jet (Bird, 2004).

2. MATHEMATICAL FORMULATION

2.1 Flow and energy equations formulation

The system in the present study is an air jet emerging into an initially stagnant air surrounding. The flow field is compressible, steady, axisymmetric and turbulent. The governing Favre-averaged transport equations can be given in the following form:

Equation of continuity:

$$\frac{\partial}{\partial x_i}(\rho u_i) = 0 \quad (1)$$

Equation of motion:

$$\frac{\partial}{\partial x_i}(\rho u_j u_i) = \frac{\partial p}{\partial x_i} + \frac{\partial}{\partial x_j} \left[\mu \left(\frac{\partial u_i}{\partial x_j} + \frac{\partial u_j}{\partial x_i} - \frac{2}{3} \delta_{ij} \frac{\partial u_l}{\partial x_l} \right) \right] + \frac{\partial}{\partial x_j} \left(-\overline{\rho u_i u_j} \right) \quad (2)$$

Equations 1 and 2 are called Reynolds-averaged Navier – Stokes (RANS) equations. Additional terms appear that represent the effects of turbulence. These Reynolds stresses $-\overline{\rho u_i u_j}$, must be modeled in order to close Equation 2. The Reynolds-averaged approach to turbulence modeling requires that the Reynolds stresses in Equation 2 be appropriately modeled. A common method employs the Boussinesq hypothesis to relate the Reynolds stresses to the mean velocity gradients:

$$\left(-\overline{\rho u_i u_j} \right) = \mu_t \left(\frac{\partial u_i}{\partial x_j} + \frac{\partial u_j}{\partial x_i} \right) - \frac{2}{3} \left(\rho k + \mu_t \frac{\partial u_l}{\partial x_l} \right) \delta_{ij} \quad (3)$$

where μ_t is the eddy viscosity, δ_{ij} is the Kronecker delta, and k is the turbulent kinetic energy per unit mass.

Energy Equation:

$$\frac{\partial(\rho C_v \tilde{T})}{\partial x_i} = -p \frac{\partial \tilde{u}_i}{\partial x_i} - p \frac{\partial \overline{u_i}}{\partial x_i} - p \frac{\partial \overline{u_i}}{\partial x_i} + \overline{\Phi} + \frac{\partial}{\partial x_i} \left(\kappa \frac{\partial T}{\partial x_i} \right) - \frac{\partial Q_i}{\partial x_i} \quad (4)$$

where κ is the thermal conductivity, \tilde{T} is the Favre average Temperature, C_v is specific heat at constant volume, $Q_i = \rho C_v u_i' T'$ and $\bar{\Phi}$ is given by:

$$\bar{\Phi} = \sigma_{ij} \frac{\partial u_i}{\partial x_j} + \sigma_{ij} \frac{\partial \overline{u_i'}}{\partial x_j} + \rho \varepsilon \quad (\text{a}) \quad \sigma_{ij} = -\frac{2}{3} \overline{\mu \frac{\partial u_k}{\partial x_k}} \delta_{ij} + \mu \left(\frac{\partial u_i}{\partial x_j} + \frac{\partial u_j}{\partial x_i} \right) \quad (\text{b}) \quad (5)$$

2.2 Turbulence Equations

The high-Reynolds number turbulent flow of technological importance contains a wide range of complex phenomena that must be modeled employing the turbulence models. Follow, are described the two turbulence models utilized in the present work, Spalart Allmaras one-equation model and v2-f four-equations model.

2.2.3 Spalart Allmaras

The transported variable in the Spalart-Allmaras model, $\tilde{\nu}$, is identical to the turbulent kinematic viscosity except in the near-wall (viscous-affected) region. The transport equation for $\tilde{\nu}$ is

$$\frac{\partial}{\partial t} (\rho \tilde{\nu}) + \frac{\partial}{\partial x_j} (\rho \tilde{\nu} u_j) = G_\nu + \frac{1}{\sigma_{\tilde{\nu}}} \left[\frac{\partial}{\partial x_j} \left\{ (\mu + \rho \tilde{\nu}) \frac{\partial \tilde{\nu}}{\partial x_j} \right\} + C_{b2} \rho \left(\frac{\partial \tilde{\nu}}{\partial x_j} \right)^2 \right] - Y_\nu + S_{\tilde{\nu}} \quad (6)$$

where G_ν is the production of turbulent viscosity and Y_ν is the destruction of turbulent viscosity that occurs in the near-wall region due to wall blocking and viscous damping. $\sigma_{\tilde{\nu}}$ and C_{b2} are constants and ν is the molecular kinematic viscosity. $S_{\tilde{\nu}}$ is a user-defined source term.

- Modeling the Turbulent Viscosity

The turbulent viscosity, μ_t is computed from:

$$\mu_t = \rho \tilde{\nu} f_{\nu 1} \quad (7)$$

where the viscous damping function, $f_{\nu 1}$, is given by

$$f_{\nu 1} = \frac{X^3}{X^3 + C_{\nu 1}^3} \quad X \equiv \frac{\tilde{\nu}}{\nu} \quad (8)$$

- Modeling the Turbulent Production

The production term, G_ν is modeled as

$$G_\nu = C_{b1} \rho \tilde{S} \tilde{\nu} \quad (9)$$

$$\text{with } \tilde{S} \equiv S + \frac{\tilde{\nu}}{k^2 d^2} f_{\nu 2} \quad f_{\nu 2} = 1 - \frac{X}{1 + X f_{\nu 1}} \quad (10)$$

C_{b1} and k are constants, d is the distance from the wall, and S is a scalar measure of the deformation tensor. By default in Fluent, as in the original model proposed by Spalart and Allmaras, S is based on the magnitude of the vorticity:

$$S \equiv \sqrt{2 \Omega_{ij} \Omega_{ij}} \quad \Omega_{ij} \text{ is the mean rate-of-rotation tensor and is defined by} \quad (11)$$

$$\Omega_{ij} = \frac{1}{2} \left(\frac{\partial u_i}{\partial x_j} - \frac{\partial u_j}{\partial x_i} \right) \quad (12)$$

- Modeling the Turbulent Destruction

The destruction term is modeled as

$$Y_D = C_{\omega 1} \rho f_{\omega} \left(\frac{\tilde{\nu}}{d} \right)^2 \quad (13)$$

where

$$f_{\omega} = g \left[\frac{1 + C_{\omega 3}^6}{g^6 + C_{\omega 3}^6} \right]^{1/6} \quad g = r + C_{\omega 2} (r^6 - r) \quad r \equiv \frac{\tilde{\nu}}{S k^2 d^2} \quad (14)$$

The standard Spalart-Allmaras model uses the distance to the closest wall as the definition for the length scale d , which plays a major role in determining the level of production and destruction of turbulent viscosity. The DES model replaces d everywhere with a new length scale \tilde{d} , defined as:

$$\tilde{d} = \min(d, C_{des} \Delta) \quad (15)$$

where the grid spacing, Δ , is based on the largest grid space in the x, y, or z directions forming the computational cell. The empirical constant C_{des} has a value of 0.65. The constants these model and of the other ones are in the Tab. 1.

2.2.4 V2-f model

An attractive alternative to the k- ϵ model is the v2-f turbulence model. The equations of v2-f model are briefly summarized below. More details are given by Durbin (1995). The turbulent viscosity is defined as:

$$\overline{v_t^2} = C_{\mu} \overline{v^2} T \quad (16)$$

and the turbulent quantities, in addition to standard k and ϵ , are obtained from two more equations: the transport equation for $\overline{v^2}$

$$U_j \frac{\partial \overline{v^2}}{\partial x_j} = k f - \frac{\overline{v^2}}{k} \epsilon + \frac{\partial}{\partial x_j} \left[\left(\nu + \frac{\nu_t}{\sigma v^2} \right) \frac{\partial \overline{v^2}}{\partial x_j} \right] \quad (17)$$

and the elliptic equation for the relaxation function f

$$L^2 \nabla^2 f - f = \frac{C_1 - 1}{T} \left(\frac{\overline{v^2}}{k} - \frac{2}{3} \right) - C_2 \frac{P_k}{\epsilon} \quad (18)$$

where the turbulence length scale L

$$L = C_L \max \left[\frac{k^{3/2}}{\epsilon}, C_{\eta} \left(\frac{\nu^3}{\epsilon} \right)^{1/4} \right] \quad (19)$$

and the turbulence time scale T

$$T = \max \left[\frac{k}{\varepsilon}, C_T \left(\frac{v}{\varepsilon} \right)^{1/2} \right] \quad (20)$$

Are bounded with their respective the Kolmogorov definitions (realisability constraints can also be applied, as given below). The constants used these model are in the Tab. 1.

Table 1. Constants of turbulence models

| Turbulence Model | Constants |
|------------------|---|
| v2-f | $C_\mu = 0.22, C_L = 0.3, C_\eta = 70.0, \alpha = 0.6, C_I = 1.4, C_2 = 0.3, C_T = 6, \sigma_{v^2} = 1$ |
| S.A. | $C_{b1} = 0.1355, C_{b2} = 0.622, \sigma_{\tilde{\nu}} = 2/3, C_{v1} = 7.1, C_{\omega1} = \frac{C_{b1}}{k^2} + \frac{(1+C_{b2})}{\sigma_{\tilde{\nu}}},$ $C_{\omega2} = 0.3, k = 0.4187$ |

3. Boundary Conditions and Computational Domain

The geometry used to modeling compressible free jet problem is shown in Fig. 2. Five boundary conditions need to be considered, including: inlet (pressure inlet), unbounded air outlet (pressure outlet) and symmetry axis.

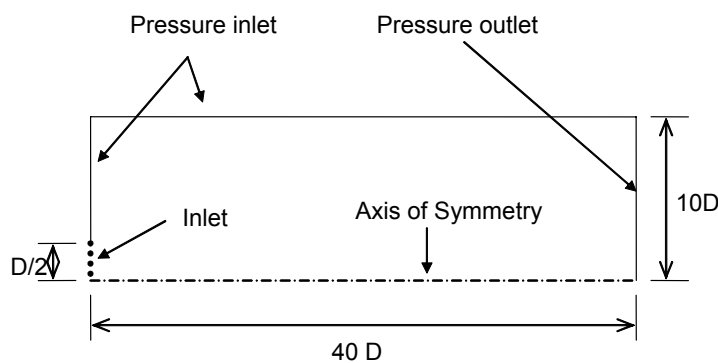


Figure 2- The solution domain and boundaries conditions

This study was focused on the Mach 0.6 axisymmetric nozzle with Reynolds number $1.7 \cdot 10^6$, Total pressure at nozzle exit 129.4 kPa, total temperature at nozzle exit 316 K, ambient pressure 101 kPa, ambient temperature 300 K and Prandtl 0.71, calculated as:

$$\text{For the total temperature at inlet } (T_{te}), \frac{T_{te}}{T_a} = 1 + \frac{k-1}{2} Ma^2 \quad (21)$$

$$\text{For the total pressure at inlet } (P_{te}), \frac{P_{te}}{P_a} = \left(1 + \frac{k-1}{2} Ma^2 \right)^{\frac{k}{k-1}} \quad (22)$$

where the sub index (a) indicates ambient condition and (te) total or stagnation condition.

Three uniform quadrilateral grid, each one with 111,400, 160,000 and 198,000 cells, were used for the grid-independence study. Fig. 3 shows the centerline decay Mach number (employing the v2-f model) for these three grids tested and are practically invariant once the deviations in the decay axial velocity from these two grid systems are less than 1% (within typical experimental error range) the grid size of 160,000 cells have been used for the rest of studies.

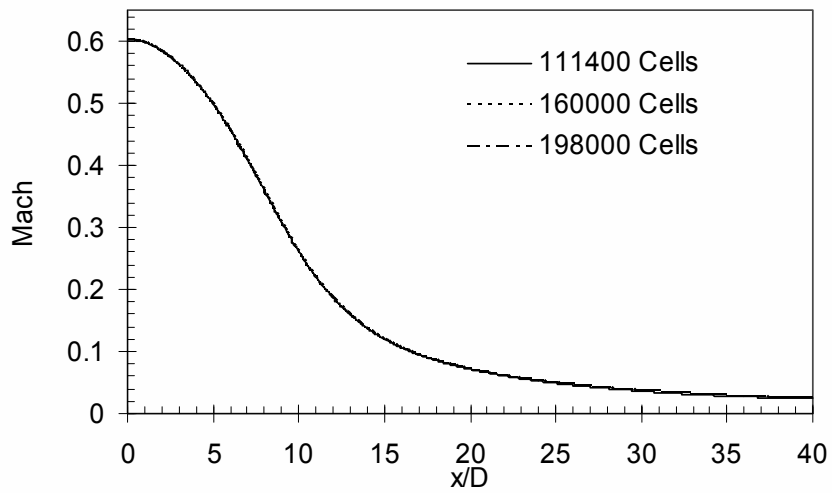


Figure 3. Profiles of Mach number along of the x dimensionless direction for three refinements, v2-f turbulence model.

The present numerical results were compared with experimental data presented in the work of Simonich et al (2001). The centerline dimensionless velocity decay (U/U_0 , U_0 = centerline velocity at nozzle exit) is shown starting from of the nozzle exit (corresponding to inlet in Fig. 2). Figures 4 and 5 show the centerline dimensionless velocity decay obtained for Spalart-Allmaras and v2-f turbulence models, respectively. As the turbulence intensity level wasn't known is the experimental test, five different turbulence levels have been specified at the inlet.

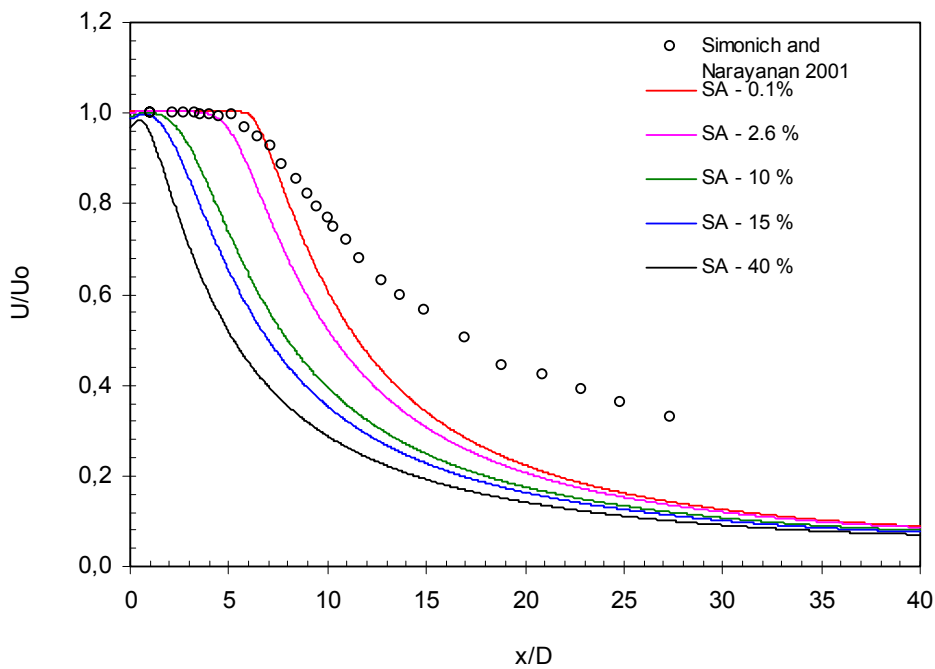


Figure 4. Centerline dimensionless velocity decay for Spallart-Almaras model.

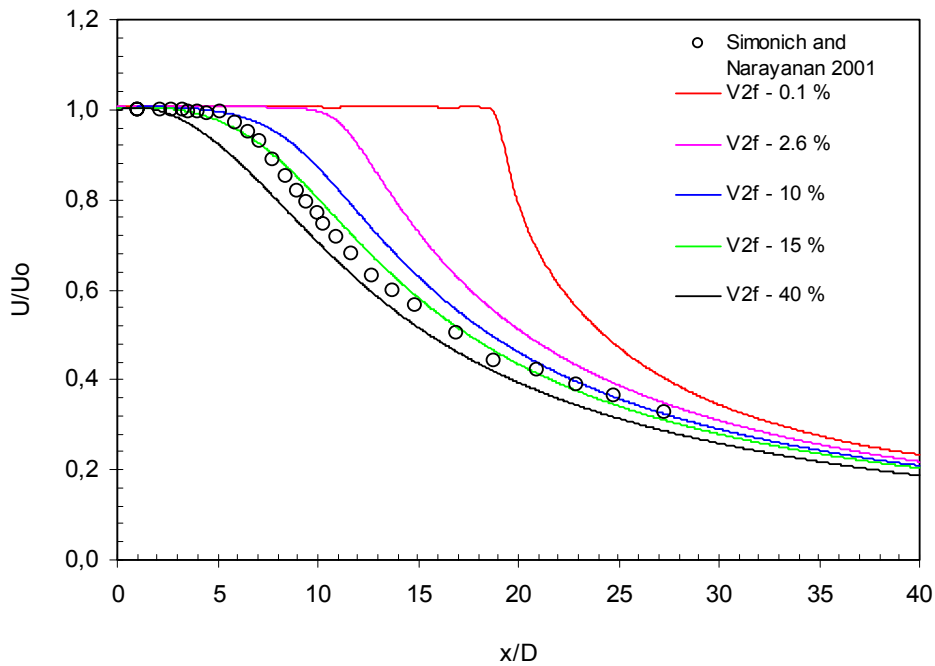


Figure 5. Centerline dimensionless velocity decay for v2-f model.

The profiles in Fig. 4 and 5 shows that for the two used turbulence models, the increase in the inlet turbulence intensity results in increase in the velocity decay rate indicating the strong dependence on the turbulent intensity level. Additionally, the Spallart Almaras model didn't agree well with the experimental data for the five tested levels of turbulence intensity as show Fig. 4. On the other hand, the v2-f model agrees satisfactory with the experimental data for intensity turbulence of 15% (see Fig. 5).

Figure 6 compares the velocity decay for the turbulence models with 15 % inlet turbulence intensity. Considerable difference has been found for the turbulence models. The Sparlat-Almaras model presented velocity decay faster over-predicting the rate mixing, while v2-f agrees well with experimental results.

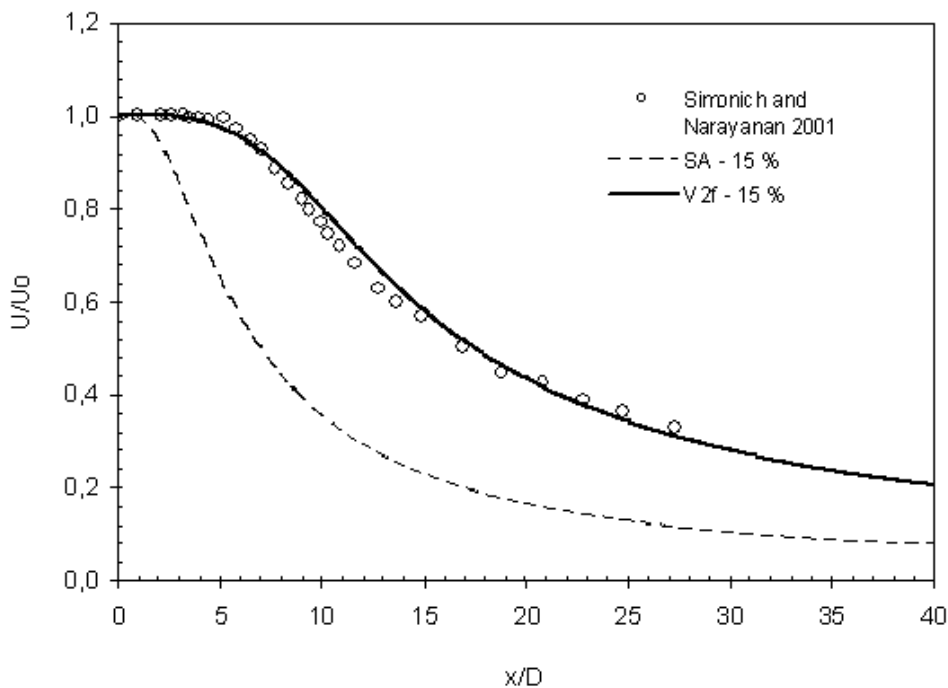


Figure 6. Centerline velocity decay for S.A. and v2-f models.

At this point, it is important to define the concept of jet spreading rate that provides a measure of jet mixing (Miller et al 1995). The jet width will increase with coordinate perpendicular to air jet outlet. The derivative of the jet width along this coordinate is known as the jet spreading rate. Just like boundary layer thickness, jet width is a quantity defined in a somewhat arbitrary way. Most authors consider jet width as the location where the axial mean velocity is 5% of its centerline value ($U \approx 0.05 U_0$). Fig. 7 shows the boundary jet spreading rate for the two turbulence models used. Note that the jet mixing of Spallar Almaras model is larger than v2-f model.

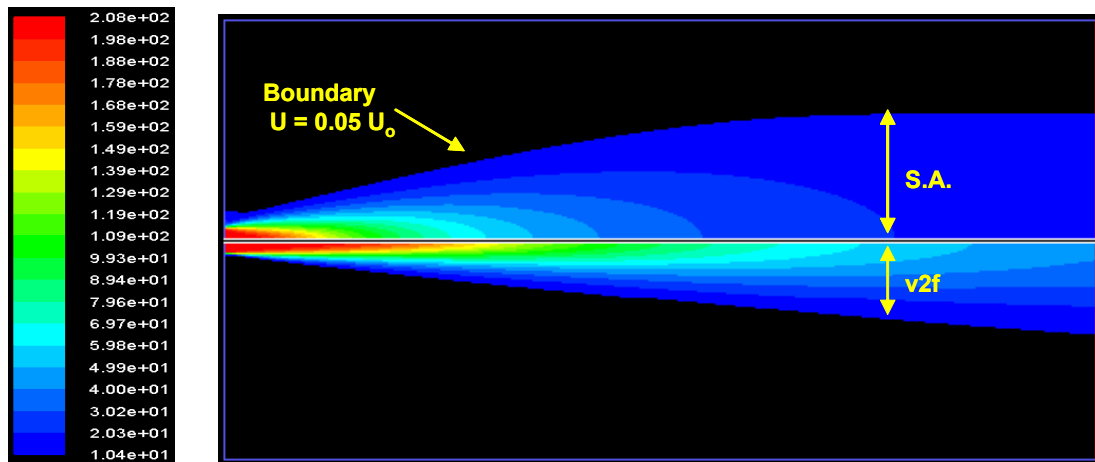


Figure 7. Comparison of boundary jet spreading rate between S.A. and v2-f turbulence models

As the v2-f model has been presented better results, this model was used to evaluate the radial decay of Mach number at seven different distances from nozzle exit, which results are given in Figure 8. It is observed that the local Mach number values are greater close to the nozzle exit than far away from it. Besides, the Mach number decay along the radial coordinate is more noticeable at the positions near the nozzle exit.

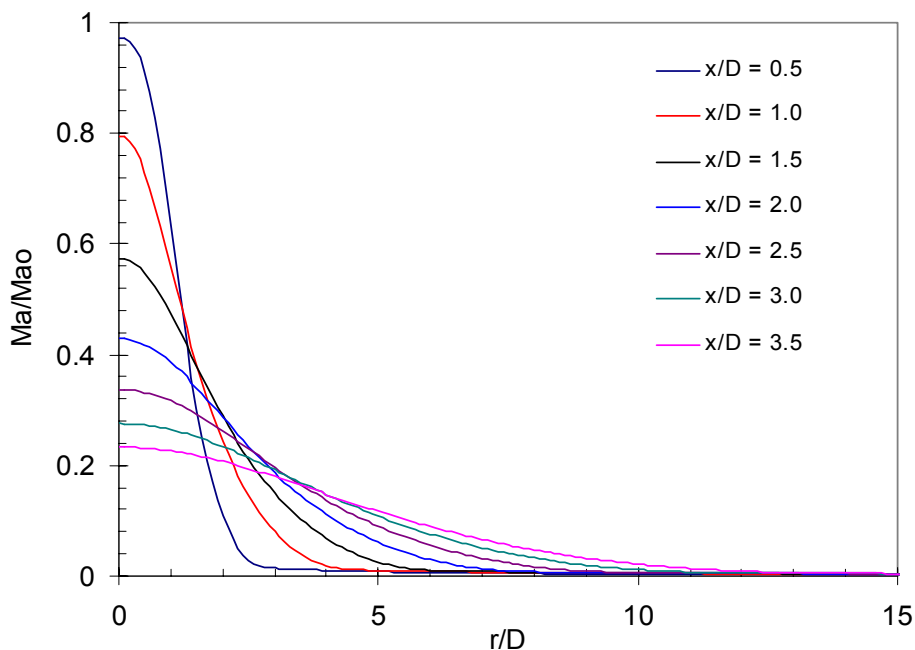


Figure 8. Radial decay of Mach number at different distances from nozzle exit, Ma_0 is the Mach number at nozzle exit.

Figures 9 and 10 depict the Mach number contours for the two turbulence models obtained using the same boundary conditions. Although these images are qualitative, it is possible to note the differences in the spreading rate provided by these two models. Again it is visible the spreading jet given by Spallar Almares model is overpredicted when compared with v2-f model. While the Mach number contour provided by v2-f model present is a thin cone (confined at the jet center region), the Spallart Almaras model presents a larger cone distribution, with the maximum (red color) restricted

close to the nozzle exit. This fact can be explained because the flow must satisfy both the energy and momentum conservation laws.

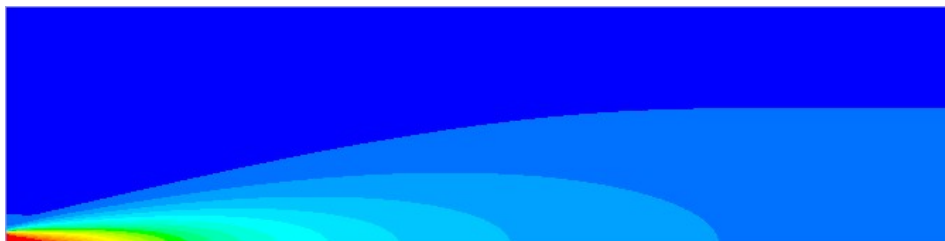


Figure 9. Mach number comparison for S.A. model – TI = 15%.

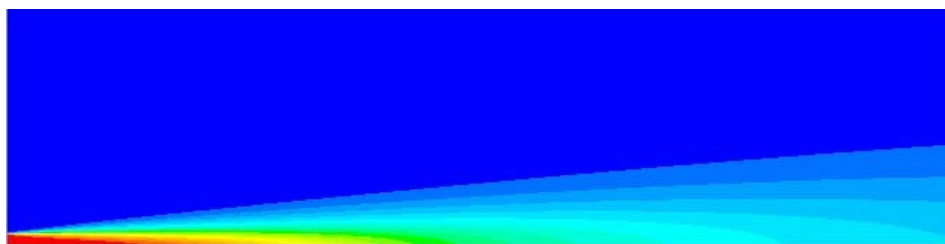


Figure 10. Mach number comparison for v2-f model – TI = 15%.

4. CONCLUSIONS

This paper presented a numerical simulation of a subsonic free jet testing two isotropic turbulence models (Spallart Almares and v2-f) using a CFD tool. Computational results of velocity were compared with the experimental data and showed that a better overall agreement was obtained employing the v2-f model. Results obtained from this investigation indicate that the free compressible jet spreading is strongly dependent on the inlet turbulence intensity level. Besides, it was shown that a suitable procedure to handle CFD commercial codes can be applied to predict reliably important fluid dynamics phenomena.

5. ACKNOWLEDGES

The authors are grateful to CNPq (grant#133598) by the support to development of this work.

6. REFERENCES

- Bird, R. B.; Stewart, W. E., 2004, "Fenômenos de Transporte", LTC Editora, 856 p.
- Durbin, P. A., 1995, "Separated Flow Computations with the k- ϵ and v2f Model". AIAA Journal, 33(4), pp. 659-664.
- M. Klein, A. Sadiki, J. Janicka, 2003, "Investigation of the influence of the Reynolds number on a plane jet using direct numerical simulation", International Journal of Heat and Fluid Flow 24, pp. 785-794.
- Miller, R. S., Madnia, C. K., and Givi, P., 1995, "Numerical Simulation of Non-Circular Jets", Comput. in Physics, Vol. 24, No. 1, pp. 1-25.
- Pais M.R. and Leland J. E., 1996, "Single-phase heat transfer characteristics of free and submerged jet impingement cooling using Mil-7808", AIAA 34th Aerospace Sciences Meeting and Exhibit, Reno, NV Jan 15-18
- Simonich J. C., Narayanan S. Barber T. J., and Nishimura M., 2001, "Aeroacoustic Characterization, Noise Reduction, and Dimensional Scaling Effects of High Subsonic Jets" AIAA Journal, v.39, n°11, pp. 2026-2069.
- Spalart, P. R. and Allmaras, S. R., 1992, "A One-Equation Turbulence Model for Aerodynamic Flows", AIAA 92-0439, AIAA 30th Aerospace Sciences Meeting, Reno, NV
- Wishart D. P. Krothapalli A., 1996, "Mean flow characteristics of a rectangular jet in a uniform stream" AIAA 34th Aerospace Sciences Meeting and Exhibit, Reno, NV Jan 15-18.